THE JOURNAL OF PHYSICAL CHEMISTRY C
A JOURNAL OF THE AMERICAN CHEMICAL SOCIETY

pubs.acs.org/JPCC

Article

Electrochemical Corrosion Inhibition of Cr_2AlC MAX Phase Coatings via Mo Solid Solution: Comprehensive Experimental and Simulation Study

Published as part of The Journal of Physical Chemistry C virtual special issue "Women Scientists in China".

Yan Zhang, Anfeng Zhang, Zhongchang Li, Zhenyu Wang,* Peiling Ke, and Aiying Wang*

Cite This: *J. Phys. Chem. C* 2024, 128, 3916−3923

Read Online

ACCESS | Metrics & More | Article Recommendations

ABSTRACT: The Cr_2AlC MAX phase has gained increasing interest as a protective coating used in harsh high-temperature oxidation and molten-salt corrosion. However, these coatings are easily apt to fail at room temperature due to the poor electrochemical corrosion resistance. Taking the concept of M-site solid solution, herein, $(Cr_{0.9}, Mo_{0.1})_2AlC$ solid solution coatings were specially fabricated by a combined technique composed of magnetron sputtering and subsequent heat treatment. The dependence of electrochemical behavior on the structural evolution was focused by comprehensive simulations and experiments. Results showed that the structure of $(Cr, Mo)_2AlC$ solid solutions was stable regardless of the Mo concentration. Moreover, compared to pristine Cr_2AlC coating, the corrosion current density was reduced and the electric impedance was enhanced by almost 1 order magnitude in 3.5 wt % NaCl solution, respectively. This was mainly ascribed to the accelerated passivation layer rich in aluminum oxides on the coating surface. Based on density functional theory simulation, the partial substitution of Mo for Cr in Cr_2AlC favored the stronger mobility of Al atoms because of the reduction in vacancy formation energy, leading to the rapid growth of passivation of aluminum oxides substantially. The observations not only provide conducive evidence of Mo solid solution for the enhanced corrosion inhibition in Cr_2AlC MAX phase coating but also offer an alternative strategy to enable the electrochemical performance of protective coatings with extended long-life serving.

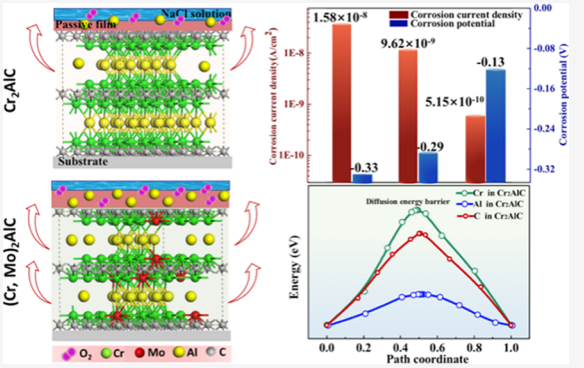

INTRODUCTION

$M_{n+1}AX_n$ phases, or "MAX phases", are a large family of ternary layered compounds that typically have weak metallic bonds between M and A atoms and covalent bonds within the $M_{n+1}X_n$ layers.[1,2] Here, M represents an early transition metal; A is an A-group element; X is either C or N, and n is a number between one and four, corresponding to the abbreviations of 211, 312, and even 413 for MAX phases. These unique nanolaminate structures and mixed bonding characteristics enable MAX phase materials to integrate the properties of metallic and ceramic materials, including superior electrical and thermal conductivity, excellent machinability, strong oxidation resistance, and corrosion resistance.[3,4] Due to such combined physiochemical advantages, MAX phases have gained increasing attention as potential protective coatings for important components that undergo harsh operating conditions like ultrahigh temperature or heavy irradiation.[5−7]

Most importantly, by substituting partial atoms on the M, A, or X sites, the mechanical, electrical, and electrochemical properties of MAX phases can be tailored and even extended for more promising utilizations. Thanks to the nanolaminate structure, the atoms located at the M position not only form strong covalent bonds with the atoms at the X position but also generate the specialized weak ionic bonds of M−A.[8,9] Therefore, M-site solid solution could vitally show a strong effect on the properties of MAX phase materials. For instance, substituting Ti with V to form a $(Ti, V)_2AlC$ solid solution significantly improved the mechanical properties of Ti_2AlC, in which the substitution led to a 29% increase in Vickers hardness, a 36% increase in flexural strength, together with a 45% increase in shear strength for $(Ti_{0.8}, V_{0.2})_2AlC$.[10] Similarly, the radiation tolerance of the Zr_3AlC_2 MAX phase was also

Received: October 20, 2023
Revised: February 4, 2024
Accepted: February 6, 2024
Published: February 21, 2024

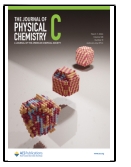

https://doi.org/10.1021/acs.jpcc.3c06948
J. Phys. Chem. C 2024, 128, 3916−3923

intensively enhanced over temperatures above 400 °C by the addition of Ti to produce $(Zr_{0.5},Ti_{0.5})_3AlC_2$ phases.[11]

Cr_2AlC, as a typical representative candidate in Al-based MAX phases, demonstrates exceptional antioxidation and corrosion resistance because of the existence of a densely protective layer rich in Al_2O_3 or $(Cr, Al)_2O_3$ during oxidation and corrosion processes.[12−17] An example was that Li et al.[12] investigated the high-temperature oxidation behavior of Cr_2AlC coatings and found the Cr_2AlC coating could effectively improve the oxidation resistance of the M38G alloy substrate. The reason was mainly ascribed to the prohibition of internal nitridation and retarded interdiffusion at the coating/substrate interface originating from the formed $(Cr, Al)_2O_3$ inner layer. In addition, once the Cr_2AlC MAX phase coating was deposited on the SS316L substrate,[18] the corrosion current density was remarkably reduced by about 2 orders of magnitude compared to the bare substrate in a mixed solution of H_2SO_4 and HF. However, it still remains a great challenge for Cr_2AlC coating to act as a protective layer with extra-strong corrosion resistance for long-term serving. Taking the concept of solid solution, M-site solid solution could be an alternatively favorable strategy to modify the electrochemical behavior of Cr_2AlC coatings without simultaneous deterioration of other excellent properties.

Generally, the most promising candidates as substitution elements are selected from those used in previously synthesized MAX phases and are adjacent to the already known elements due to similar atomic size and electronic structure. One observation was that the substitution of Mn for Cr in the Cr_2AlC system, where the magnetic properties could be changed in a wide range with increasing Mn solubility.[19,20] Meantime, in our previous work,[21] a significant reduction in the friction coefficient and wear rate was obtained in $(Cr, V)_2AlC$ coatings, in which the V replaced Cr in the composition ranging from 19 to 47 atom %. Considering the difference in atoms, a solid solution of Mo to the Cr_2AlC matrix would offer a more pronounced effect on physiochemical properties compared to using V and Mn because Mo is also adjacent to Cr but belongs to the same main group. As a result, this work aims to investigate the structural stability and electrochemical behavior of $(Cr, Mo)_2AlC$ solid solution by comprehensive theoretical calculations and experimental analysis.

METHODS

Atomic-Scale Calculations. The present study utilized the CAmbridge Sequential Total Energy Package (CASTEP)[22,23] to conduct theoretical simulation of $(Cr, Mo)_2AlC$ solid solutions via the density functional theory (DFT) based on the plane−wave pseudopotential method. The generalized gradient approximation constructed by Perdew−Burke−Ernzerhof[24] was specially adopted for the exchange-correlation energy functional. The choice of k points in the Brillouin zone and the plane-wave cutoff energy are empirically determined through the convergence test. In this case, the plane-wave cutoff energy is primarily set to be 480 eV, and the determined k points are around 5 × 5 × 2, enabling the energy accuracy within 1 meV/atom. Meantime, a 2 × 2 × 1 supercell with 32 atoms was built to simulate the characteristics of vacancy defects. Such a supercell size is enough adequate to mode the MAX phase due to the relatively small number of atoms in a unit cell (8 atoms).[25] Afterward, the self-diffusion barrier of each atom along the basal plane in the Cr_2AlC phase was calculated by searching the transition state linking the two end defective configurations using the LST/QST method, which generally combined the linear (LST) or quadratic synchronous transit (QST) methods with conjugate gradient refinements.[26]

Fabrication of Coatings. For comparison, Cr_2AlC and $(Cr, Mo)_2AlC$ coatings were fabricated on Ti-6Al-4 V substrates using a magnetron sputtering deposition system input with multiple targets, followed by vacuum annealing. The rectangular $Cr_{1.5}Al$ compound target (produced by powder metallurgical process) and a molybdenum target (purity: 99.99 wt %) with the same size at 400 mm × 100 mm × 7 mm were co-sputtered in the coating deposition, where the hybrid gas mixtures composing of CH_4 with a flow rate at 3 sccm and Ar gas at a flow rate of 100 sccm acted as the reactive precursors during sputtering. Prior to deposition, the substrates were ultrasonically cleaned with alcohol for 15 min and then placed in the deposition chamber. The sample was fixed to a rotational substrate holder in front of the $Cr_{1.5}Al$ target at a distance of about 12 cm. During deposition, the current applied to the $Cr_{1.5}Al$ target and Mo target were 3 and 0.6 A, respectively. The process was lasted for 3 h at a deposition temperature of 150 °C. After deposition, the as-prepared coatings were annealed at 550 °C for 1.5 h under a vacuum pressure of 3.0×10^{-4} Pa to obtain $(Cr, Mo)_2AlC$ MAX phases. Details of a similar deposition system could be seen in the reference 21.

Electrochemical Behavior Measurements. Electrochemical behavior including potentiodynamic and potentiostatic measurements were carried out by the Gamry electrochemical workstation in a standard three-electrode configuration. The test specimens with an effective working area of ∼0.2 cm^2, platinum wire, and Ag/AgCl electrode were used as the working electrode, counter electrode, and reference electrode, respectively. The working electrolyte of 3.5 wt % NaCl solution was served to simulate the marine corrosive environment. Before testing, each test specimen was immersed in the electrolyte solution for 60 min to stabilize open circuit potential. Relevant corrosion resistance was analyzed by a potentiodynamic polarization curve recorded from −0.5 to 1.5 V at a scanning rate of 1 mV/s. In order to figure out the dependence of anticorrosion behavior on passivation films, the potentiostatic tests were finally undertaken at +0.5 V for 6 h. The electrochemical impendence spectroscopy (EIS) tests were finished at potentiostatic mode with a perturbation voltage of 10 mV in the frequency range of 100 kHz to 10 mHz. Various electrochemical parameters were achieved by fitting EIS via Zview software on the basis of suitable equivalent circuits.

Microstructural Characterization Methods. The phase formation of solid solution coatings was investigated by X-ray diffraction (XRD, Bruker D8 Advance, Germany) with Cu Kα radiation (λ = 0.154 nm). Surface morphology and chemical composition of the coatings were characterized by scanning electron microscopy (SEM, FEI Quanta FEG 250) equipped with an energy-dispersive X-ray spectrometer (EDS). Furthermore, transmission electron microscopy (TEM, Talos F200X) was used to further elucidate the microstructure characteristics of coatings, where the samples for the TEM test were specially prepared by a focused ion beam technique.

https://doi.org/10.1021/acs.jpcc.3c06948
J. Phys. Chem. C 2024, 128, 3916−3923

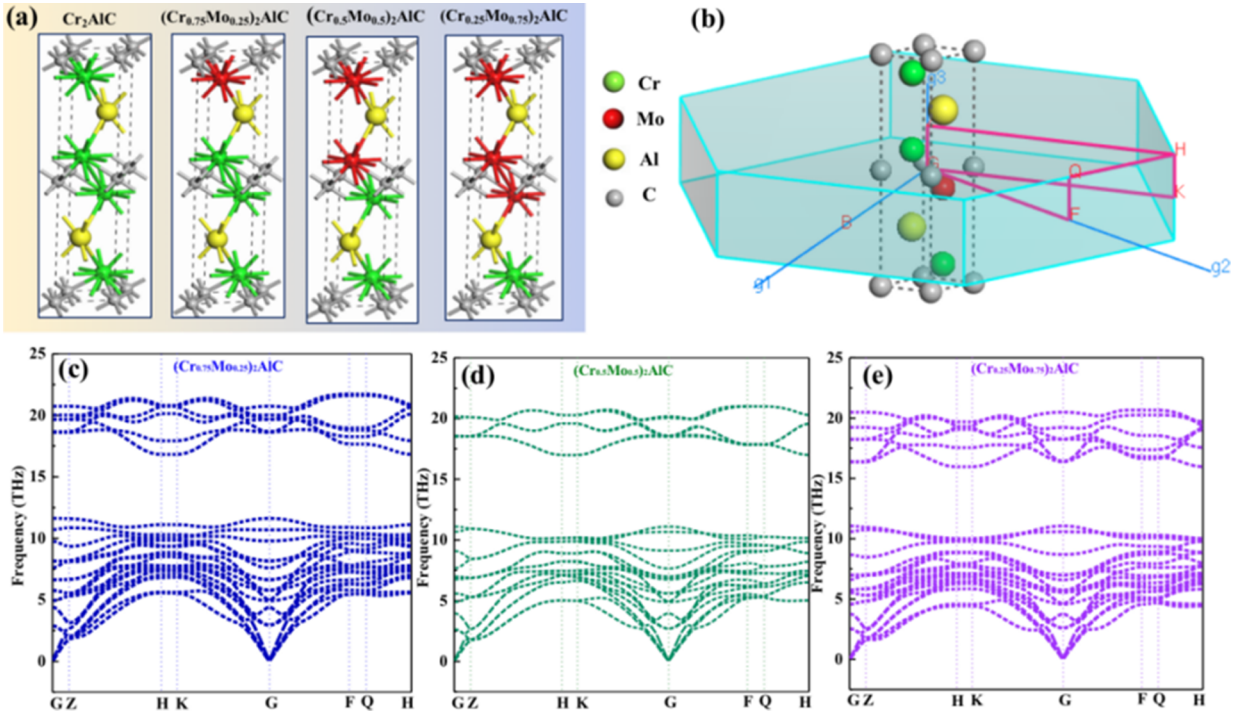

Figure 1. (a) Crystal structure of $(Cr, Mo)_2AlC$ with different Mo contents. (b) First Brillouin zone and special k-paths. (c–e) Phonon spectra of $(Cr, Mo)_2AlC$.

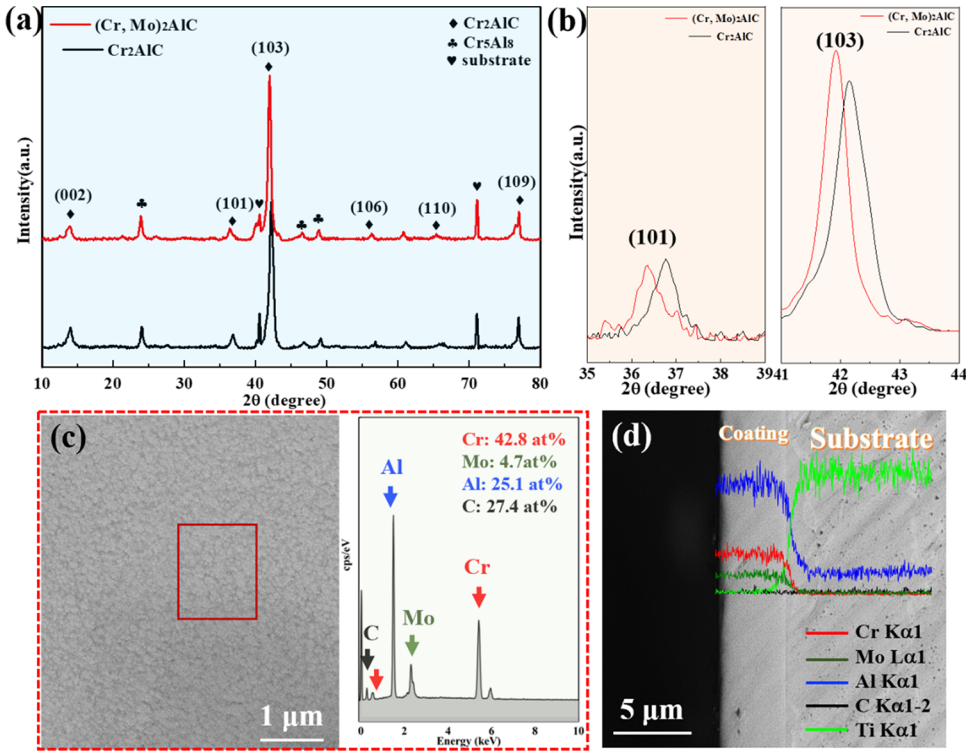

Figure 2. (a) XRD images of the prepared coatings. (b) Enlarged view of the selected angle range. (c) Surface morphology of the coating and the corresponding EDS results. (d) Cross-sectional image and EDS line scanning of the coating.

RESULTS AND DISCUSSION

Structural Stability of Solid Solution Coating. It is empirically known that the Cr_2AlC MAX phase presents a hexagonal structure with a space group of $P6_3/mmc$ ($a = b =$ 0.286 nm, $c =$ 1.282 nm).[27] To investigate the structural stability in Cr_2AlC with the M-site Mo solid solution, phonon band structures were simulated by the aforementioned DFT methods. Figure 1a shows the corresponding structural models of $(Cr, Mo)_2AlC$ with various Mo contents, corresponding to the representative cases of $(Cr_{0.75}, Mo_{0.25})_2AlC$, $(Cr_{0.5}, Mo_{0.5})_2AlC$, and $(Cr_{0.25}, Mo_{0.75})_2AlC$. The related first Brillouin zone and the special k-paths employed in the phonon

https://doi.org/10.1021/acs.jpcc.3c06948
J. Phys. Chem. C 2024, 128, 3916−3923

calculation are indicated in Figure 1b. After calculations, Figure 1c−e displays the phonon spectra of the $(Cr, Mo)_2AlC$ system with different Mo contents by solid solution. It turns out that despite the peaks in the high-frequency domain (about 15−20 THz), all the studied coatings possess similar phonon spectra. Since the lattice vibration could be deduced from these spectra, the stability of each crystal structure was then evaluated. It was clear that no any virtual frequencies emerged at any wave vector in the whole Brillouin zone for all phases studied, indicating the atoms in the crystal were stable at their equilibrium positions.[28] This result essentially identified the dynamical stabilization of formed crystal structures in the $(Cr, Mo)_2AlC$ solid solutions regardless of the Mo concentration.

Growth and Structure of $(Cr, Mo)_2AlC$ Coatings. Figure 2a shows the comparative XRD spectra for the fabricated Cr_2AlC coatings with and without a Mo solid solution. The XRD patterns illustrated the detectable crystalline phases for both samples, which could be assigned to the dominant Cr_2AlC phase based on the standard PDF card No. 00-029-0017. Particularly, introducing the Mo element to the Cr_2AlC matrix as an M-site solid solution caused the shifting downward of diffraction peaks compared to that of the pristine Cr_2AlC coating. The distinct evidence could be found in the local enlarged image of XRD spectra (Figure 2b), where the peaks at around 37 and 42° could be originated from the (101) plane and (103) plane of Cr_2AlC coating, respectively. With this aspect, it could be said that the high-purity $(Cr, Mo)_2AlC$ solid solution coating was successfully synthesized by the hybrid process composed of a pristine deposited Cr−Mo−Al-C coating and a subsequent thermal annealing. The reason behind this peak shifting could be ascribed to the larger atomic radius of Mo (1.36 Å) than that of Cr (1.25 Å), accompanying an increase in the lattice constants and consequently the corresponding interplanar spacings. Representatively, Figure 2c shows the surface morphology together with the elemental distribution in the $(Cr, Mo)_2AlC$ solid solution coating. Similar to the previous Cr_2AlC coating,[18,29] a homogeneous and dense structure was achieved for the solid solution coating. Moreover, the relevant EDS results confirmed that the atomic ratio of (Cr + Mo)/Al was 1.9, namely, with Cr-42.8 atom %, Mo-4.7 atom %, Al-25.1 atom %, and C-27.4 atom %, supporting the specialized formation of $(Cr_{0.9}, Mo_{0.1})_2AlC$ solid solution coating. The EDS line scanning along the cross-sectional image (Figure 2d) revealed the uniform distribution of Cr, Mo, Al, and C elements during the coating growth, where a strong adherent interface without visible cracks was found between the coating layer and substrate as well.

The structural characteristics of the $(Cr_{0.9}, Mo_{0.1})_2AlC$ solid solution MAX phase were further addressed through high-resolution transmission electron microscopy (HRTEM). The apparent observation was that the coating demonstrated a very dense microstructure with distinctly equiaxed crystals (Figure 3a), in which the lattice fringes with interplanar spacings of 2.524 and 0.958 Å could be assigned to the (100) plane and (213) plane (Figure 2b), respectively. It was noticeable that these *d*-spacings were larger than those of the pure Cr_2AlC planes (relevant to 2.468 and 0.915 Å),[30] mainly due to the substitution of Mo for Cr atoms. To further examine the distribution of the Cr, Mo, Al, and C components, aberration-corrected HAADF-EDX mapping was performed. As shown in Figure 3c, the analysis results suggested a uniform distribution for all Cr, Mo, Al, and C components in the coating, which agreed well with the SEM-EDS results. As evidence, the

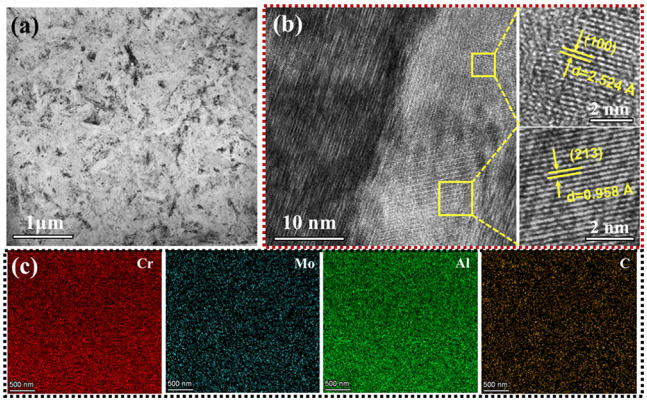

Figure 3. TEM and HADDF-EDX mapping images of the $(Cr, Mo)_2AlC$ layer: (a) bright-field image, (b) HRTEM image, and (c) HADDF-EDX element mapping of Cr, Mo, Al, and C.

synthesis of high-purity $(Cr_{0.9}, Mo_{0.1})_2AlC$ solid solution MAX phase coatings with fine equiaxed grains was successfully fabricated in this study.

Electrochemical Properties of $(Cr, Mo)_2AlC$ Coatings. Figure 4 presented the potentiodynamic polarization curves of the $(Cr_{0.9}, Mo_{0.1})_2AlC$ solid solution coating, Cr_2AlC coating, and bare Ti-6Al-4 V in a 3.5 wt % NaCl solution for comparison, as well as the calculated electrochemical properties based on Tafel extrapolation fitting correspondently. It was visible that both Cr_2AlC MAX phase coating with and without Mo solid solution significantly enhanced the corrosion resistance compared to the bare substrate. In particular, the calculated corrosion current densities (I_{corr}) of solid solution coating were about 5.15×10^{-10} A/cm^2, approximately 1 and 2 orders of magnitude lower than those of Cr_2AlC coating and substrate, respectively. Meanwhile, the corrosion potentials (E_{corr}) were about −0.13, −0.29, and −0.33 V for the $(Cr, Mo)_2AlC$, Cr_2AlC coating, and bare Ti-6Al-4 V, respectively. In general, the value of I_{corr} was proportional to the corrosion rate of materials, while the higher E_{corr} represented the difficulty in corrosion tendency.[31,32] It could be thus concluded that even both the $(Cr, Mo)_2AlC$ coating and Cr_2AlC coating improved the corrosion resistance of the Ti-6Al-4 V substrate, and the coating with Mo solid solution possessed the best corrosion inhibition performance. Furthermore, according to the values of I_{corr} and E_{corr}, the kinetics of the corrosion reactions could later be deduced.

In an attempt to understand the corrosion evolution of $(Cr_{0.9}, Mo_{0.1})_2AlC$ solid solution coating in simulated 3.5 atom % NaCl solution, the samples were analyzed in detail by EIS measurements. All EIS measurements were carried out once the specialized stability condition was achieved. As shown in Figure. 5a, all the coatings exhibited a larger radius of the capacitance loop compared to the uncoated Ti-6Al-4 V substrate. This observation could be related to the enhancement of the electrochemical corrosion resistance and capacitive behavior for the solid/liquid interface. Since these EIS spectra could be subsequently fitted by suitable equivalent circuits, the kinetic reactions during the corrosion process could thus be deduced. For the used circuits, R_s was solution resistance, Q_f and R_t were electrical double-layer capacitor and charge transfer resistance, Q_f and R_f were assigned to passive layer capacitance and resistance, respectively. In addition, a constant phase element was employed instead of capacitance to simulate the inhomogeneous surface.[33] Table 1 summarizes the

https://doi.org/10.1021/acs.jpcc.3c06948
J. Phys. Chem. C 2024, 128, 3916−3923

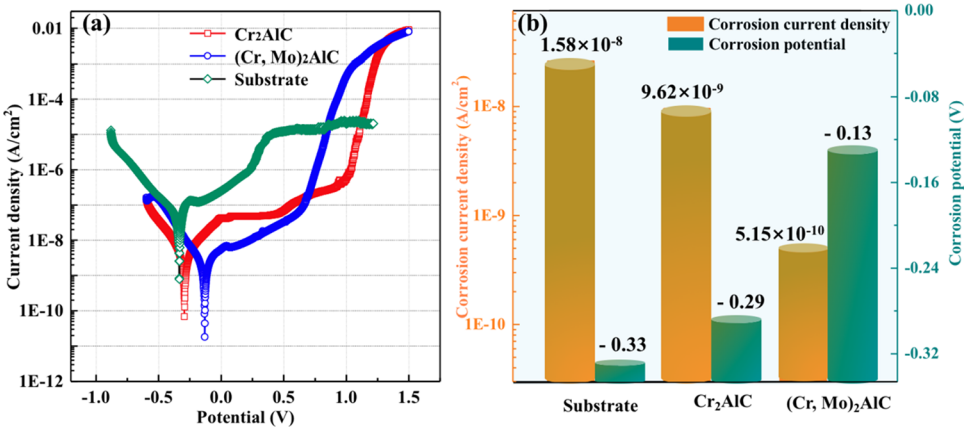

Figure 4. (a) Potentiodynamic polarization curves of $(Cr, Mo)_2AlC$, Cr_2AlC coating, and bare Ti-4Al-4 V in 3.5 wt % NaCl solution. (b) Corrosion current densities and corrosion potentials.

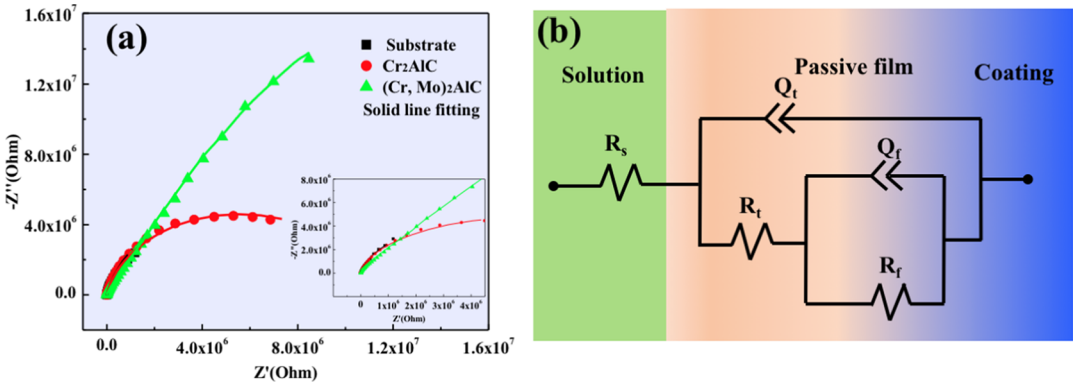

Figure 5. (a) Nyquist plots of tested samples at open circuit potentials in 3.5 wt % NaCl solution. (b) Equivalent circuit of EIS plots.

Table 1. Electrochemical Parameters by Fitting EIS of the Specimen in Stimulated NaCl Solution

specimens	R_s Ω cm^{-2}	Q_t F cm^{-2}	R_t Ω cm^{-2}	Q_f F cm^{-2}	R_f Ω cm^{-2}
Ti-6Al-4 V	13.80	4.37×10^{-6}	1.36×10^{2}	1.97×10^{-5}	1.21×10^{6}
Cr_2AlC coating	56.19	6.02×10^{-7}	1.18×10^{4}	2.81×10^{-7}	1.01×10^{7}
$(Cr_{0.9}, Mo_{0.1})_2AlC$ coating	56.71	1.82×10^{-7}	3.81×10^{4}	1.35×10^{-7}	7.82×10^{8}

electrochemical parameters extracted from the equivalent circuit. The value of R_f for each tested specimen was significantly higher than that of R_t, indicating the strong dependence of corrosion resistance upon ionic transportation within the formed passive layer. Moreover, compared to the bare substrate, the higher R_f values obtained in Cr_2AlC and $(Cr, Mo)_2AlC$ coatings presented the improvement of anticorrosion capability. One achievement was that the value of R_f with Mo solid solution was about 7.82×10^8 Ω/cm^2, which was much larger than that of the substrate at 1.21×10^6 Ω/cm^2 and Cr_2AlC coating at 1.01×10^7 Ω/cm^2. This was consistent with the polarization analysis, illustrating that the addition of the Mo element distinctly enhanced the corrosion durability related to the passive film.

Evolution of Passivation Film on Coating Surface. Previous studies[34−38] introduced the consistent observations on the excellent oxidation and corrosion resistance in MAX phases with A-site Al element, because of the easier formation of a dense aluminum oxide layer on the surface. Currently, the relevant microstructure evolution of the passive layer was performed for the solid solution coating after potentiostatic polarization at +0.5 V for 6 h. Figure 6a shows the cross-sectional morphology of the $(Cr_{0.9}, Mo_{0.1})_2AlC$ coating as well as the corresponding EDS profiles for the various elements. There was a clear presence of a formed passive layer over the coating surface, beyond of the used protective carbon layer during the test. The elemental distribution extracted from EDS images also indicated that the passive film was enriched in Cr, Al, and O elements. Notably, the Al concentration was remarkably higher than that of Cr, identifying that the passive film was dominated by aluminum oxides, in accordance with previous studies.[39,40] Most importantly, the thickness of the generated passive film in the $(Cr_{0.9}, Mo_{0.1})_2AlC$ coating was about 50 nm, larger than that of the Cr_2AlC coating at ∼35 nm (Figure 6b,c). This strengthened passivation could account for the improvement of corrosion resistance by Mo solid solution.

To elucidate the key role of Mo solid solution on corrosion behavior of Cr_2AlC coating, a DFT simulation was conducted to understand the atomic-scale evolution of the passive layer emerging on the coating surface. Particularly, the formation and transportation of individual atomic vacancy in the Cr_2AlC MAX phase were simulated using the CASTEP software

https://doi.org/10.1021/acs.jpcc.3c06948
J. Phys. Chem. C 2024, 128, 3916−3923

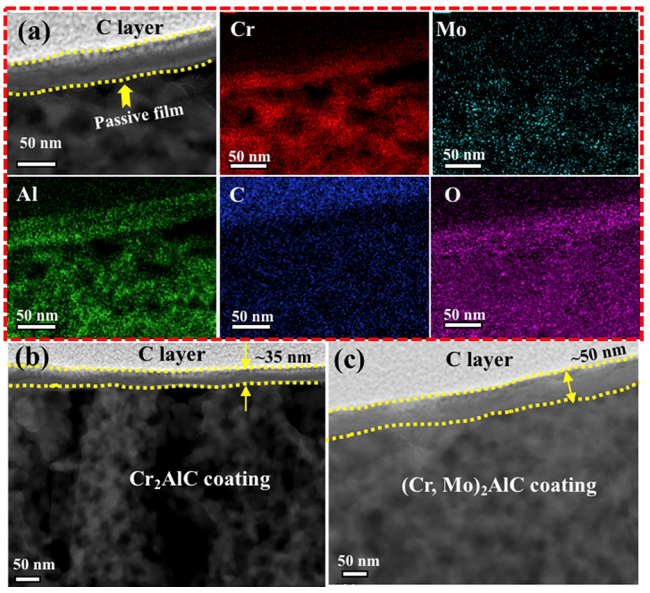

Figure 6. (a) Cross-sectional of $(Cr, Mo)_2AlC$ coating and the corresponding EDS results. STEM-HAADF images of (b) Cr_2AlC coating and (c) $(Cr, Mo)_2AlC$ coating.

package in the framework of DFT. The vacancy formation energies of Cr, Al, and C in the Cr_2AlC supercells were calculated to be 1.975 2.287, and 6.823 eV, respectively. In this aspect, the formation energies were in the sequence of $\Delta E_C < \Delta E_{Al} < \Delta E_{Cr}$, implying that both Cr vacancy and Al vacancy were favorable monovacancies in defective Cr_2AlC structure compared to the C vacancies. Since the existence of vacancy for each atom in Cr_2AlC was strongly dependent upon the atom mobility, we further simulated the migration energy, assuming the specialized atom diffusion in Cr_2AlC structure occurred through sublattice-diffusion together with neighbored vacancy jumping along the basal plane. Figure 7a shows the migration energy for Cr, Al, and C in Cr_2AlC, which were approximately 3.89 0.46, and 2.54 eV, respectively. It could be apparent that the diffusion energy barrier of the Al atom in the Cr_2AlC was much lower than that for Cr and C,[41] which would enable the preferential reaction of Al atoms with exposed oxygen to form an aluminum oxide passive film over the coating surface. Furthermore, once the Mo atom was introduced to Cr_2AlC as an M-site solid solution element, the vacancy formation energy for Al atoms in the substituted compounds was monotonically reduced with increasing Mo content (Figure 7b). According to this achievement, the evidence was clear that additive Mo elements significantly favored the higher mobility of Al atoms by decreasing the formation energy. Consequently, the growth rate of passivation film in $(Cr_{0.9}, Mo_{0.1})_2AlC$ solid solution coating was accelerated, whereby the thickness of passivation film in $(Cr_{0.9}, Mo_{0.1})_2AlC$ coating reached to 50 nm approximately, while it was only 35 nm for Cr_2AlC coating (Figure 6b,c).

For a more detailed understanding, Figure 8 illustrates a schematic for the dependence of corrosion behavior on the

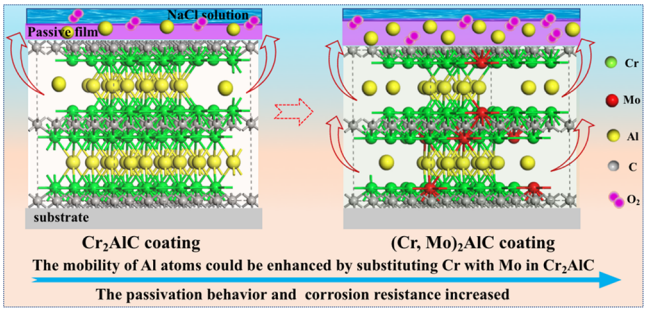

Figure 8. Schematic mechanism for the comparative corrosion inhibition of Cr_2AlC MAX phase coating with and without Mo solid solution in 3.5 wt % NaCl solution.

electrochemical activities in Cr_2AlC coating with and without Mo solid solution comparatively. For the pristine high-purity Cr_2AlC coated Ti-6Al-4 V substrate, the Al atoms behaved with a lower diffusion barrier than those of Cr and C atoms, which enabled the preferential reaction of Al atoms with exposed oxygen in 3.5 atom % NaCl solution. Subsequently, the appearance and growth of aluminum oxide was dominated in the passivation film, contributing to the enhanced corrosion resistance of Cr_2AlC coating. An example was that the corrosion current density was reduced by about one order in Cr_2AlC coating than that of the bare substrate. However, once the Mo solid solution was evolved in the Cr_2AlC MAX phases, the mobility of Al atoms located in the nanolaminate lattices was significantly accelerated along the basal plane due to the reduction of formation energy. These in turn promoted the adequate migration of Al outward to the coating surface in a solid solution structure, subsequently accounting for the rapid growth of the passive layer. As a result, the corrosion current

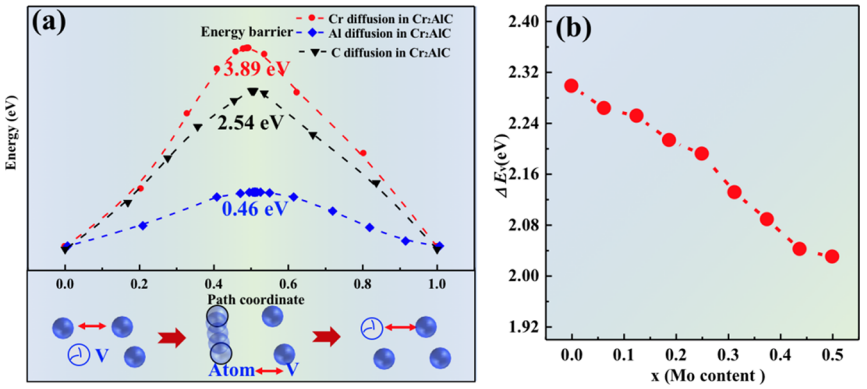

Figure 7. Formation energy of a monovacancy in Cr_2AlC. (a) Migration energy of each atomic vacancy. (b) Calculated formation energy of an Al vacancy in $(Cr, Mo)_2AlC$ supercells.

https://doi.org/10.1021/acs.jpcc.3c06948
J. Phys. Chem. C 2024, 128, 3916−3923

density in $(Cr_{0.9}, Mo_{0.1})_2AlC$ coating was reduced by about 2 orders of magnitude than that of the substrate, accompanied with the massive upsurge of corrosion potential being 3 times larger simultaneously. Evidently, the thickness of the passivation film in $(Cr_{0.9}, Mo_{0.1})_2AlC$ coating reached 50 nm approximately, while it was only 35 nm for Cr_2AlC coating. The consistent results revealed that the corrosion inhibition properties of Cr_2AlC coatings were remarkably enhanced by the conception of a Mo solid solution under harsh chloride solution at room temperature.

CONCLUSIONS

In this study, high-purity $(Cr_{0.9}, Mo_{0.1})_2AlC$ solid solution MAX phase coatings were successfully fabricated via a hybrid magnetron sputtering technique, together with subsequent vacuum annealing. The dependence of the microstructural evolution upon the electrochemical behavior of coatings in 3.5 wt % NaCl solution was focused by combined experiments and atomic-scale simulations. Compared to pristine Cr_2AlC MAX phase coating, introducing Mo solid solution in MAX phases could significantly improve the corrosion inhibition properties in a chloride environment. Particularly, the $(Cr_{0.9}, Mo_{0.1})_2AlC$ coating exhibited the lowest corrosion current density around 5.15×10^{-10} A/cm^2 and the highest corrosion potential being −0.13 V compared with those of Cr_2AlC coating and bare Ti-6Al-4 V substrate. With the aid of the existence of Mo atoms, the elemental distribution after the potentiostatic polarization test revealed that the generation of a passivation layer enriched with aluminum oxides was remarkably accelerated on the coating surface. According to the DFT simulations, the reason behind this observation could be attributed to the mobility changes of Al atoms in the nanolaminate MAX phase relevant to the Mo solid solution. Specifically, the partial substitution of Mo for Cr in Cr_2AlC favored the higher mobility of Al atoms in the lattice, leading to the rapid growth of passivation aluminum oxides with a thickness of about 50 nm. Most importantly, increasing Mo concentration in the Cr_2AlC matrix could distinctly reduce the formation energy of Al vacancy, accounting for the increase of the passivation film arising from migration activity of Al atoms in corrosive solution for $(Cr, Mo)_2AlC$ coating with various Mo concentrations. The result not only identified that substituting Cr with Mo in Cr_2AlC coating was conducive to enhancing the corrosion inhibition properties of MAX phase coatings in harsh NaCl solution but also brought forward the promising strategy to modify the electrochemical performance of protective coatings by taking the conception of solid solution associated with vacancy defects.

AUTHOR INFORMATION

Corresponding Authors

Zhenyu Wang − *Key Laboratory of Marine Materials and Related Technologies, Zhejiang Key Laboratory of Marine Materials and Protective Technologies, Ningbo Institute of Materials Technology and Engineering Chinese Academy of Sciences, Ningbo 315201, China*; Email: wangzy@nimte.ac.cn

Aiying Wang − *Key Laboratory of Marine Materials and Related Technologies, Zhejiang Key Laboratory of Marine Materials and Protective Technologies, Ningbo Institute of Materials Technology and Engineering Chinese Academy of Sciences, Ningbo 315201, China; Center of Materials Science and Optoelectronics Engineering, University of Chinese Academy of Sciences, Beijing 100049, China*; orcid.org/0000-0003-2938-5437; Email: aywang@nimte.ac.cn

Authors

Yan Zhang − *Key Laboratory of Marine Materials and Related Technologies, Zhejiang Key Laboratory of Marine Materials and Protective Technologies, Ningbo Institute of Materials Technology and Engineering Chinese Academy of Sciences, Ningbo 315201, China*

Anfeng Zhang − *Key Laboratory of Marine Materials and Related Technologies, Zhejiang Key Laboratory of Marine Materials and Protective Technologies, Ningbo Institute of Materials Technology and Engineering Chinese Academy of Sciences, Ningbo 315201, China; Center of Materials Science and Optoelectronics Engineering, University of Chinese Academy of Sciences, Beijing 100049, China*

Zhongchang Li − *Key Laboratory of Marine Materials and Related Technologies, Zhejiang Key Laboratory of Marine Materials and Protective Technologies, Ningbo Institute of Materials Technology and Engineering Chinese Academy of Sciences, Ningbo 315201, China; Center of Materials Science and Optoelectronics Engineering, University of Chinese Academy of Sciences, Beijing 100049, China*

Peiling Ke − *Key Laboratory of Marine Materials and Related Technologies, Zhejiang Key Laboratory of Marine Materials and Protective Technologies, Ningbo Institute of Materials Technology and Engineering Chinese Academy of Sciences, Ningbo 315201, China; Center of Materials Science and Optoelectronics Engineering, University of Chinese Academy of Sciences, Beijing 100049, China*

Complete contact information is available at: https://pubs.acs.org/10.1021/acs.jpcc.3c06948

Notes

The authors declare no competing financial interest.

ACKNOWLEDGMENTS

This research was supported by the National Science Found for Distinguished Young Scholars of China (52025014), the National Natural Science Foundation of China (52171090 and U22A20111), the Director's Fund of Ningbo Institute of Materials Technology and Engineering, Chinese Academy of Sciences (2022SZKY0308), the Zhejiang Province Selected Funding for Postdoctoral Research Projects (ZJ2023106), and the Zhejiang Provincial Natural Science Foundation (Q24E010013).

REFERENCES

(1) Barsoum, M. W. The $M_{N+1}AX_N$ phases: A new class of solids: Thermodynamically stable nanolaminates. *Progress in solid state chemistry* **2000**, *28* (1−4), 201−281.

(2) Tao, Q.; Lu, J.; Dahlqvist, M.; Mockute, A.; Calder, S.; Petruhins, A.; Meshkian, R.; Rivin, O.; Potashnikov, D.; Caspi, E. A.; et al. Atomically layered and ordered rare-earth i-MAX phases: a new class of magnetic quaternary compounds. *Chem. Mater.* **2019**, *31* (7), 2476−2485.

(3) Khazaei, M.; Bae, S.; Khaledialidusti, R.; Ranjbar, A.; Komsa, H.-P.; Khazaei, S.; Bagheri, M.; Wang, V.; Mochizuki, Y.; Kawamura, M.; et al. Superlattice MAX Phases with A-Layers Reconstructed into 0D-Clusters, 1D-Chains, and 2D-Lattices. *J. Phys. Chem. C* **2023**, *127* (30), 14906−14913.

(4) Li, T.; Chao, F.; Yue-Ming, L.; Xiao-Xing, F.; En-Ge, W.; Guo-Rui, Z. MAX phase: synthesis, structure and property. *Prog. Phys.* **2021**, *41* (1), 39.

(5) Wang, Z.; Sun, J.; Xu, B.; Liu, Y.; Ke, P.; Wang, A. Reducing the self-healing temperature of Ti_2AlC MAX phase coating by substituting Al with Sn. *Journal of the European Ceramic Society* **2020**, *40* (1), 197−201.
(6) Sun, Z. M. Progress in research and development on MAX phases: a family of layered ternary compounds. *International Materials Reviews* **2011**, *56* (3), 143−166.
(7) Eklund, P.; Beckers, M.; Jansson, U.; Högberg, H.; Hultman, L. The $M_{n+1}AX_n$ phases: Materials science and thin-film processing. *Thin Solid Films* **2010**, *518* (8), 1851−1878.
(8) Näslund, L.; Persson, P. O.; Rosen, J. X-ray Photoelectron Spectroscopy of Ti_3AlC_2, Ti_3C_2Tz, and TiC Provides Evidence for the Electrostatic Interaction between Laminated Layers in MAX-Phase Materials. *J. Phys. Chem. C* **2020**, *124* (50), 27732−27742.
(9) Wang, J.; Zhou, Y. Dependence of elastic stiffness on electronic band structure of nanolaminate M_2AlC (M= Ti, V, Nb, and Cr) ceramics. *Phys. Rev. B* **2004**, *69* (21), No. 214111.
(10) Meng, F.; Zhou, Y.; Wang, J. Strengthening of Ti_2AlC by substituting Ti with V. *Scripta materialia* **2005**, *53* (12), 1369−1372.
(11) Bowden, D.; Ward, J.; Middleburgh, S.; de Moraes Shubeita, S.; Zapata-Solvas, E.; Lapauw, T.; Vleugels, J.; Lambrinou, K.; Lee, W.; Preuss, M.; Frankel, P. The stability of irradiation-induced defects in Zr_3AlC_2, Nb_4AlC_3 and $(Zr_{0.5}, Ti_{0.5})_3AlC_2$ MAX phase-based ceramics. *Acta Mater.* **2020**, *183*, 24−35.
(12) Li, J.; Xiang, H.; Xu, J.; Zheng, L.; Qian, Y. Oxidation and cracking behaviors of triple-layered Cr_2AlC coating. *Surf. Coat. Technol.* **2021**, *422*, No. 127554.
(13) Chen, X.; Stelzer, B.; Hans, M.; Iskandar, R.; Mayer, J.; Schneider, J. M. Enhancing the high temperature oxidation behavior of Cr_2AlC coatings by reducing grain boundary nanoporosity. *Materials Research Letters* **2021**, *9* (3), 127−133.
(14) Wang, Z.; Ma, G.; Liu, L.; Wang, L.; Ke, P.; Xue, Q.; Wang, A. High-performance Cr_2AlC MAX phase coatings: Oxidation mechanisms in the 900−1100 °C temperature range. *Corros. Sci.* **2020**, *167*, No. 108492.
(15) Pradeep, K.; Chang, K.; Kovács, A.; Sen, S.; Marshal, A.; de Kloe, R.; Dunin-Borkowski, R.; Schneider, J. Nano-scale Si segregation and precipitation in $Cr_2Al(Si)C$ MAX phase coatings impeding grain growth during oxidation. *Materials Research Letters* **2019**, *7* (5), 180−187.
(16) Li, J.; Qian, Y.; Niu, D.; Zhang, M.; Liu, Z.; Li, M. Phase formation and microstructure evolution of arc ion deposited Cr_2AlC coating after heat treatment. *Appl. Surf. Sci.* **2012**, *263*, 457−464.
(17) Wang, Q.; Renteria, A. F.; Schroeter, O.; Mykhaylonka, R.; Leyens, C.; Garkas, W.; to Baben, M. Fabrication and oxidation behavior of Cr_2AlC coating on Ti6242 alloy. *Surf. Coat. Technol.* **2010**, *204* (15), 2343−2352.
(18) Ma, G.; Zhang, D.; Guo, P.; Li, H.; Xin, Y.; Wang, Z.; Wang, A. Phase orientation improved the corrosion resistance and conductivity of Cr_2AlC coatings for metal bipolar plates. *J. Mater. Sci. Technol.* **2022**, *105*, 36−44.
(19) Mockuté, A.; Lu, J.; Moon, E.; Yan, M.; Anasori, B.; May, S.; Barsoum, M.; Rosén, J. Solid solubility and magnetism upon Mn incorporation in the bulk ternary carbides Cr_2AlC and Cr_2GaC. *Materials Research Letters* **2015**, *3* (1), 16−22.
(20) Mockute, A.; Persson, P. O.; Magnus, F.; Ingason, A. S.; Olafsson, S.; Hultman, L.; Rosen, J. Synthesis and characterization of arc deposited magnetic $(Cr, Mn)_2AlC$ MAX phase films. *Phys. Status Solidi (RRL)* **2014**, *8* (5), 420−423.
(21) Wang, Z.; Wang, C.; Zhang, Y.; Wang, A.; Ke, P. M-site solid solution of vanadium enables the promising mechanical and high-temperature tribological properties of Cr_2AlC coating. *Materials & Design* **2022**, *222*, No. 111060.
(22) Groden, K.; Vila, F. D.; Li, L.; Bare, S. R.; Scott, S. L.; McEwen, J.-S. First-Principles Approach to Extracting Chemical Information from X-ray Absorption Near-Edge Spectra of Ga-Containing Materials. *J. Phys. Chem. C* **2021**, *125* (51), 27901−27908.
(23) Segall, M.; Lindan, P. J.; Probert, M. A.; Pickard, C. J.; Hasnip, P. J.; Clark, S.; Payne, M. First-principles simulation: ideas, illustrations and the CASTEP code. *J. Phys.: Condens. Matter* **2002**, *14* (11), 2717.
(24) Perdew, J. P.; Burke, K.; Ernzerhof, M. Generalized gradient approximation made simple. *Physical review letters* **1996**, *77* (18), 3865.
(25) Ting, L.; Wang, J. Y.; Zhou, Y. C. Ab initio modeling of the formation and migration of monovacancies in Ti_2AlC. *Script. Mater.* **2008**, *59* (2), 854−857.
(26) Govind, N.; Petersen, M.; Fitzgerald, G.; King-Smith, D.; Andzelm, J. A generalized synchronous transit method for transition state location. *Computational materials science* **2003**, *28* (2), 250−258.
(27) Huang, Q.; Han, H.; Liu, R.; Lei, G.; Yan, L.; Zhou, J. Saturation of ion irradiation effects in MAX phase Cr_2AlC. *Acta Mater.* **2016**, *110*, 1−7.
(28) Wen, M.; Chen, X.; Zheng, Z.; Deng, S.; Li, Z.; Wang, W.; Chen, H. In-plane anisotropic Raman spectroscopy of van der Waals α-MoO_3. *J. Phys. Chem. C* **2021**, *125* (1), 765−773.
(29) Yuan, J.; Zhou, S.; Wu, H.; Wang, Z.; Zhang, Y.; Zhou, G.; Ma, G.; Ke, P.; Wang, A. Ultrahigh strength-ductility of nanocrystalline Cr2AlC coating under micropillar compression. *Scripta Materialia* **2023**, *235*, No. 115594.
(30) Schneider, J. M.; Sun, Z.; Mertens, R.; Uestel, F.; Ahuja, R. Ab initio calculations and experimental determination of the structure of Cr_2AlC. *Solid State Commun.* **2004**, *130* (7), 445−449.
(31) Mao, A.; Ding, P.; Quan, F.; Zhang, T.; Ran, X.; Li, Y.; Jin, X.; Gu, X. Effect of aluminum element on microstructure evolution and properties of multicomponent Al-Co-Cr-Cu-Fe-Ni nanoparticles. *J. Alloys Compd.* **2018**, *735*, 1167−1175.
(32) Starosvetsky, D.; Gotman, I. Corrosion behavior of titanium nitride coated Ni−Ti shape memory surgical alloy. *Biomaterials* **2001**, *22* (13), 1853−1859.
(33) Sathiyanarayanan, S.; Azim, S. S.; Venkatachari, G. A new corrosion protection coating with polyaniline−TiO_2 composite for steel. *Electrochim. Acta* **2007**, *52* (5), 2068−2074.
(34) Shi, H.; Azmi, R.; Han, L.; Tang, C.; Weisenburger, A.; Heinzel, A.; Maibach, J.; Stüber, M.; Wang, K.; Müller, G. Corrosion behavior of Al-containing MAX-phase coatings exposed to oxygen containing molten Pb at 600 °C. *Corros. Sci.* **2022**, *201*, No. 110275.
(35) Wang, Z.; Ma, G.; Li, Z.; Ruan, H.; Yuan, J.; Wang, L.; Ke, P.; Wang, A. Corrosion mechanism of Ti_2AlC MAX phase coatings under the synergistic effects of water vapor and solid NaCl at 600 C. *Corros. Sci.* **2021**, *192*, No. 109788.
(36) Li, X.; Xie, X.; Gonzalez-Julian, J.; Malzbender, J.; Yang, R. Mechanical and oxidation behavior of textured Ti_2AlC and Ti_3AlC_2 MAX phase materials. *Journal of the European Ceramic Society* **2020**, *40* (15), 5258−5271.
(37) Zhang, Z.; Chai, J.; Jin, H.; Pan, J.; Wong, L. M.; Lim, S. H.; Sullivan, M. B.; Wang, S. J. Oxidation of single crystalline Ti_2AlN thin films between 300 and 900 °C: a perspective from surface analysis. *J. Phys. Chem. C* **2016**, *120* (33), 18520−18528.
(38) Li, S.; Xiao, L.; Song, G.; Wu, X.; Sloof, W. G.; van der Zwaag, S. Oxidation and crack healing behavior of a fine-grained Cr_2AlC ceramic. *J. Am. Ceram. Soc.* **2013**, *96* (3), 892−899.
(39) Li, X.; Wang, S.; Wu, G.; Zhou, D.; Pu, J.; Yu, M.; Wang, Q.; Sun, Q. Oxidation and hot corrosion behaviors of MAX-phase Ti_3SiC_2, Ti_2AlC, Cr_2AlC. *Ceram. Int.* **2022**, *48* (18), 26618−26628.
(40) Tang, C.; Große, M.; Ulrich, S.; Klimenkov, M.; Jäntsch, U.; Seifert, H. J.; Stüber, M.; Steinbrück, M. High-temperature oxidation and hydrothermal corrosion of textured Cr_2AlC-based coatings on zirconium alloy fuel cladding. *Surf. Coat. Technol.* **2021**, *419*, No. 127263.
(41) Ling, W. D.; Wei, P.; Zhao, D. Q.; Shao, Y. P.; Duan, J. Z.; Han, J. F.; Duan, W. S. First principles investigation of mono-vacancy defective properties of Cr_2AlC. *Physica B: Condensed Matter* **2019**, *552*, 178−183.

https://doi.org/10.1021/acs.jpcc.3c06948
J. Phys. Chem. C 2024, 128, 3916−3923